

Inferring ecological interactions from time series data using neural ordinary differential equations fitted by gradient matching

Willem Bonnaffé^{1,2}, Ben Sheldon¹, & Tim Coulson²

1. Edward Grey Institute of Field Ornithology, Department of Zoology, Oxford University, Zoology Research and Administration Building, 11a Mansfield Road, Oxford OX1 3SZ

2. Ecological and Evolutionary Dynamics Lab, Department of Zoology, Oxford University, Zoology Research and Administration Building, 11a Mansfield Road, Oxford OX1 3SZ

Emails: willem.bonnafe@stx.ox.ac.uk; tim.coulson@zoo.ox.ac.uk

Running title: Repeatable interactions and dynamics

Keywords: Artificial Neural Networks; Ecological Dynamics; Ecological interactions; Geber Method; Neural Ordinary Differential Equations; Ordinary Differential Equations; Prey-predator dynamics; Time series analysis; Rotifers; Microcosm;

Specifications: 140 words in abstract; 7071 words in text; 40 references; 5 figures; 1 table

Contact: Willem Bonnaffé, 61 St Giles, Pusey House, St Cross College, Oxford, OX1 3LZ, UK (w.bonnafe@gmail.com)

Statement of authorship: Willem Bonnaffé designed the method, performed the analysis, wrote the manuscript; Ben Sheldon provided input for the manuscript, commented on the manuscript. Tim Coulson led investigations, provided input for the manuscript, commented on the manuscript.

Abstract

Generalisation of dynamical processes across natural systems is difficult because they are complex and hard to observe. The hope is that generalisation may be achieved by adequately modelling the complexity of systems, and observe them in sufficient detail. We investigate this by looking at the consistency of ecological interactions across three replicates of a three-species prey-predator system, well-observed in an artificial environment, using neural ordinary differential equations. We find that dominant interactions are consistent across the replicates, while weaker interactions are not, leading to different dynamical patterns across replicated systems. Our study hence suggests that generalisation of dynamical processes across systems may not be possible, even in simpler systems in ideal monitoring conditions. This is a problem because if we are not able to make generalisations in a simple artificial system, how can we make generalisation in the real world?

1 Introduction

The repeatability of ecological and evolutionary dynamics varies widely across systems and species. Sticklebacks from different lakes in Canada have independently evolved to a similar river morph phenotype (Thompson, Taylor, and Mcphail 1997). In guppies, four replicated populations located in different streams in Trinidad evolved the same low-predation phenotype (Reznick, Bryga, and Endler 1990). Multiple studies in experimental microcosms, particularly in rotifer populations, have shown that population dynamics were broadly repeatable (Yoshida et al. 2003; Yoshida et al. 2007; Becks et al. 2010; Becks et al. 2012; Hiltunen et al. 2013). Overall, this demonstrated that ecological and evolutionary dynamics may be repeatable across different instances of the same system, at least qualitatively. This was a fascinating finding given the complexity of the mechanisms involved and the subtle variations in environmental conditions across the different populations.

These systems hinted at the possibility for identifying global, generalisable, dynamical models. In practice, however, generalising dynamics and dynamical processes (i.e. functional representations describing which and how state variables affect each other and determine system dynamics) across natural systems has proven difficult (Lawton 1999). First, even if the dynamical patterns, and their outcomes, may appear to be conserved across similar systems, they may be underpinned by different processes. For instance, the evolution of the sticklebacks to highly similar river-adapted phenotypes has been shown to be underpinned by radically different genetic alterations (Raeymaekers et al. 2017). Second, it is often unclear whether quantitative differences across replicated systems

21 arise from pure stochasticity (Dallas et al. 2021), observation error (De Meester et al. 2019), or
22 deterministic changes in the dynamical processes. Finally, the complexity of biological processes
23 themselves (Adamson and Morozov 2013), differences in genetic and environmental contexts, may
24 prevent the identification of a suitable dynamical model. For example, Becks and colleagues found
25 that differences in the initial amount of genetic variation in otherwise identical rotifer populations
26 led to subtle changes to the dynamics (Becks et al. 2010). Different access to seed supplies can
27 modify the strength of the interaction between a plant and its herbivore, leading to either stable or
28 oscillatory dynamics (Bonsall, Van Der Meijden, and Crawley 2003). Differences in temperature
29 can alter the ecological interaction structure of entire ecosystems (Shurin et al. 2012; Bonnaffé
30 et al. 2021). Because of this, vital rates are often found to be inconsistent in time (Gross, Ives, and
31 Nordheim 2005; Adamson and Morozov 2013), and space (e.g. Gamelon et al. 2019). Overall, a
32 growing body of evidence shows that generalisation of dynamical processes across similar natural
33 systems often fails (Lawton 1999, e.g. Kendall et al. 2005; Demyanov, Wood, and Kedwards 2006;
34 Ezard, Côté, and Pelletier 2009).

35 So how could repeatable dynamics arise across multiple instances of the same system? We would
36 expect dynamics to be repeatable if the components of the system (e.g. species), as well as interac-
37 tions between components, are conserved. For this, populations should have similar distributions
38 for the traits that underpin these interactions, and should further share the same environmental con-
39 ditions, across instances. While this is unreasonable to expect from a natural system, it may be
40 achievable in an artificial setting. In such a setting, it is possible to understand the structure of

41 the system, to control the environment, and to reduce observation error. So if we fail to identify
42 and generalise dynamical models in natural systems, perhaps we may be able to do so in artificial
43 systems.

44 In spite of this there are few studies that have attempted to characterise the generalisability of
45 dynamics across replicated systems in a laboratory setting. In such a setting, idiosyncrasies in pop-
46 ulation dynamics can arise from (1) variations in ecological interactions and individual processes,
47 as a result of evolution (e.g. Yoshida et al. 2003), or stochasticity (Dallas et al. 2021), (2) variations
48 in initial conditions due to the experimental setting (Yoshida et al. 2003; Becks et al. 2010; De
49 Meester et al. 2019), and (3) the complexity of the system which can lead to large changes in sys-
50 tem dynamics with small changes in the system state and structure (Adamson and Morozov 2013).

51 Two studies, one in aphids and the other in rotifers, found substantial variation in vital rates across
52 replicated populations, by fitting a stage-structured population ODE model to population dynamics
53 time series data (Bruijning, Jongejans, and Turcotte 2019; Rosenbaum et al. 2019). These studies
54 hint that generalisability of population dynamical processes may not be possible because of in-
55 trinsic population structure and evolution, even in virtually identical populations hosted in artificial
56 environments.

57 We identified three gaps in the literature. First, this kind of evidence remains scarce, due in part
58 to the fact that dynamical modelling approaches guided by empirical data are still not widespread
59 (Pontarp, Brännström, and Petchey 2019). Second, most of these studies relied on parametric
60 frameworks, which impose arbitrary pre-determined forms for the dynamical processes at play, so

61 that their model may not capture properly the complexity of the dynamics of these populations (Jost
62 and Ellner 2000; Adamson and Morozov 2013; Bonnaffé, Sheldon, and Coulson 2021). Finally,
63 most studies usually analyse dynamics in single-species systems, but not multi-species systems,
64 such as those with intraguild predation, which are more biologically realistic scenarios (Hiltunen
65 et al. 2013). Further studies are consequently required to investigate the consistency of dynamical
66 processes in simple multi-species and well-observed systems, to conclude about the generalisability
67 of population dynamics across systems.

68 Our aim in this study is to provide an assessment of the repeatability of dynamical processes across
69 different instances of a realistic multi-species system hosted in a well-observed environment. We
70 do this by quantifying the direction, strength, and consistency of interactions in time and across
71 replicates of a three-species microcosm in an experimental setting. We hypothesise that if the
72 system is (1) simple enough, (2) well-observed, (3) in a controlled environment, then dynamical
73 effects/interactions should be broadly consistent in time and across replicates, hence allowing for
74 generalisation of dynamics across systems. We consider three replicates of a three-species system,
75 consisting in a prey (algae), intermediate-predator (flagellate), and top-predator (rotifer). The algae
76 is consumed by the flagellate and rotifer, and the flagellate is consumed by the rotifer. We use
77 three replicated system runs from a study by Hiltunen and colleagues which feature sequential
78 oscillations of the density of the three species (Hiltunen et al. 2013). We analyse the time series
79 with neural ordinary differential equations (Bonnaffé, Sheldon, and Coulson 2021), which allows
80 us to approximate non-parametrically population growth rates, and quantify the direction, strength,

81 and consistency of inter- and intra-specific effects on the growth of each population. We find that
82 the interaction between the rotifer and algae is consistent throughout time and across replicates,
83 while the interaction between the flagellate and the two other species is not. Our study suggests
84 that dynamical processes may sometimes not be consistent and generalisable across systems, even
85 when they are as close to identical as experimentation permits. We discuss these results and hint at
86 the underlying impact of evolution driving differences in these systems.

87 **2 Material and Methods**

88 **2.1 Method overview**

89 We aim to provide a nonparametric method for estimating ecological interactions from time series
90 data of species density. We do this by approximating the dynamics of each species with neural
91 ordinary differential equations (NODEs, Bonnaffé, Sheldon, and Coulson 2021). We then compute
92 ecological interactions as the sensitivity of these dynamics to a change in the respective species
93 densities.

94 **2.2 Neural ordinary differential equation**

95 A NODE is a class of ordinary differential equation (ODE) that is partly or entirely defined as an
96 artificial neural network (ANN). They are useful to infer dynamical processes non-parametrically
97 from time series data (Bonnaffé, Sheldon, and Coulson 2021). We choose NODEs over standard
98 statistical approaches because they offer two advantages. The first is that NODEs approximate

the dynamics of populations non-parametrically. NODEs are therefore not subjected to incorrect model specifications (Jost and Ellner 2000; Adamson and Morozov 2013). This provides a more objective estimation of the inter-dependences between state variables. The second advantage is that it is a dynamical systems approach. So that the approach includes lag effects through interacting state variables, not only direct effects between them.

We first consider a multi-species NODE system,

$$\frac{dN_i}{dt} := r_i(N, \Theta_i) N_i \quad (1)$$

where dN_i/dt denotes the change in the density of i^{th} species, $N_i \in \mathcal{R}^+$, in continuous time, as a function of the density of other species $N = \{N_1, N_2, \dots, N_I\}$. The per-capita growth rate r_i is a non-parametric function of the density of each species. The shape of the non-parametric function is controlled by the parameter vectors Θ_i . In the context of NODEs, each non-parametric function is defined as an ANN function of the state variables. The most common class of ANN used for NODEs are single layer perceptrons (SLPs),

$$r_i(N, \Theta_i) := \theta^{(0)} + \sum_{j=1}^J \theta_j^{(1)} f_\sigma \left(\theta_j^{(2)} + \sum_{k=1}^K \theta_{jk}^{(3)} N_k \right) \quad (2)$$

which feature a single layer that maps the inputs, here the species densities N , to a single output, the per-capita growth rate of the focal population r_i . The parameter vector Θ_i contains the weights $\theta_{jk}^{(l)}$ of the connections in the SLPs. SLPs can be viewed as weighted sums of activation functions

114 f_{σ} . More details regarding these models can be found in our previous work (Bonnaiffé, Sheldon,
115 and Coulson 2021).

116 **2.3 Fitting NODEs by gradient matching**

117 This section describes how to estimate the parameters β of the NODE system given a set of time
118 series. In previous work, we developed a simulation-based approach to fit NODE systems to time
119 series data (Bonnaiffé, Sheldon, and Coulson 2021). We would first simulate the NODE system over
120 the entire time series. Then we would compute the error between the predictions of the NODE
121 model and the observations. Finally, we would change the weights of the NODEs to minimise
122 this error. There are two caveats with this approach. The first caveat is that the NODE system
123 has to be simulated over the entire range of the data at every step of the optimisation. This step is
124 computationally expensive to perform. Second, the numerical integration prevents the computation
125 of gradients of the posterior distribution of the model. This prevents the use of efficient gradient
126 descent approaches.

127 Instead, we propose to use a *gradient matching* approach to fit NODEs, which relies on data in-
128 terpolation to approximate states and dynamics. The method we propose here is derived from the
129 *gradient matching* approach that Ellner and colleagues developed to fit ODEs (Ellner, Seifu, and
130 Smith 2002; Wu, Fukuhara, and Takeda 2005). We proceed in three steps, presented graphically in
131 Fig. 1 and detailed in the following sections. First, we interpolate the time series data and dynamics
132 of each species in the system. Second, we train each NODE to satisfy the interpolated dynamics,

133 thereby avoiding the simulation step of the previous method.

134 **Data interpolation**

135 We interpolate the time series and differentiate it with respect to time in order to approximate
 136 the dynamics of the system. We perform the interpolation via non-parametric regression of the
 137 interpolating function on the time series data,

$$\varepsilon_{it}^{(o)}(\Omega_i | n_{it}) := n_{it} - \tilde{N}_i(t, \Omega_i) \quad (3)$$

138 where the observation error, $\varepsilon_{it}^{(o)}$, is defined as the difference between the observed value of the
 139 variable at time t , n_{it} , and the value predicted by the interpolating function $\tilde{N}_i(t, \Omega_i)$. The interpo-
 140 lating function is chosen to be a SLP,

$$\tilde{N}_i(t, \Omega_i) := \exp \left\{ \omega^{(0)} + \sum_{j=1}^J \omega_j^{(1)} f_{\sigma} \left(\omega_j^{(2)} + \omega_j^{(3)} t \right) \right\} \quad (4)$$

141 where $\tilde{N}(t, \Omega_i)$ is the interpolated state variable, defined as a weighted sum of activation functions
 142 of time. The interpolation parameter vector Ω_i contains the weights ω of the SLP. If $f_{\sigma} := \sin$, then
 143 the weights $\omega_j^{(1)}$, $\omega_j^{(2)}$, and $\omega_j^{(3)}$ control the amplitude, shift, and frequency of the oscillations in
 144 the time series, respectively. Following this approach we obtain directly an approximation of the
 145 dynamics of the state variable by differentiating the SLP with respect to time,

$$\frac{\partial \tilde{N}_i}{\partial t}(t, \Omega_i) = \sum_{j=1}^J \omega_j^{(1)} \omega_j^{(3)} \frac{\partial f_{\sigma}}{\partial t} \left(\omega_j^{(2)} + \omega_j^{(3)} t \right) \tilde{N}_i(t, \Omega_i) \quad (5)$$

146 **Fitting NODEs to interpolated data**

147 In a second step, we train the NODE system (1) to satisfy the interpolated dynamics. Thanks to the
 148 interpolation step, this simply amounts to performing a non-parametric regression of each NODE
 149 (equation 1) on the interpolated dynamics (equation 5),

$$\varepsilon_{it}^{(p)}(\Theta_i | \Omega) := \frac{\partial \tilde{N}_i}{\partial t}(t, \Omega_i) - \frac{dN_i}{dt}(\tilde{N}, \Theta_i) \quad (6)$$

150 where the process error, $\varepsilon_{it}^{(p)}$, is defined as the difference between the interpolated dynamics $\partial \tilde{N}_i / \partial t$
 151 and the NODE dN_i / dt , given the interpolated state variables \tilde{N} .

152 **Statistical modelling**

153 It is already possible at this stage to fit the NODE system (1) to the time series via standard op-
 154 timisation. First, we could interpolate the data by finding the parameter vector Ω that minimises
 155 the observation error $\varepsilon^{(o)}$ in equation (3). Second, we could fit the NODEs by finding the param-
 156 eter vector Θ that minimises the process error $\varepsilon^{(p)}$ in equation (6). However, in this study, we use
 157 Bayesian regularisation in order to control for over-fitting (Cawley and Talbot 2007), and to root
 158 our interpretation of uncertainty in a statistically sound framework.

159 First, we define the model to fit the interpolating functions to the time series data. We assume
 160 normal distributions for the observation error, $\varepsilon_{ij}^{(o)} \sim \mathcal{N}(0, \sigma_i)$, and for the prior density of the
 161 parameters, $\Omega_{ij} \sim \mathcal{N}(0, \gamma_{ij})$. For the interpolation, we are only interested in fitting the time series
 162 accurately, irrespective of the value of σ_i and γ_{ij} . So we perform inference on the second level, by

163 optimising the marginal posterior distribution. To do this, we use the approach developed by Caw-
 164 ley and Talbot to average out the value of the parameters σ_i and γ_{ij} in the full posterior distribution
 165 (Cawley and Talbot 2007), assuming gamma hyperpriors $p(\xi) \propto \frac{1}{\xi} \exp\{-\xi\}$ for both parameters.
 166 This yields the following expression for the log marginal posterior density of the parameters,

$$\log P(\Omega_i | N_i) \propto -\frac{J}{2} \log \left(1 + \sum_{j=1}^J \left(\varepsilon_{ij}^{(o)} \right)^2 \right) - \frac{K}{2} \log \left(1 + \sum_{k=1}^K \Omega_{ik}^2 \right) \quad (7)$$

167 where P denotes the marginal posterior distribution, N_i corresponds to the observed density of
 168 species i , J is the total number of time steps in the time series, $\varepsilon_{ij}^{(o)}$ is the observation error at
 169 time step j for species i , K is the total number of parameters. More details on how to derive this
 170 expression can be found in a supplementary file (Supplementary A).

171 Then, we define the model to fit the NODEs to the interpolated dynamics, given the interpolated
 172 states. We assume normal distributions for the observation error, $\varepsilon_{ij}^{(p)} \sim \mathcal{N}(0, \sigma_i)$, and for the
 173 prior density of the parameters, $\Theta_{jk} \sim \mathcal{N}(0, \delta_{jk})$. This gives the following expression for the log
 174 posterior distribution of the parameters given the interpolations,

$$\log p(\Theta_i | \Omega) \propto -\frac{1}{2} \sum_{j=1}^J \left(\frac{\varepsilon_{ij}^{(p)}}{\sigma_i} \right)^2 - \frac{1}{2} \sum_{k=1}^K \left(\frac{\Theta_{ik}}{\delta_{ik}} \right)^2 \quad (8)$$

175 where Ω corresponds to the interpolation parameters of all interpolated state variables, $\varepsilon_{ij}^{(p)}$ is the
 176 process error at time step j for species i , σ_i is the standard deviation of the likelihood, K is the total
 177 number of parameters, δ_{ik} is the standard deviation of the prior distribution of parameter Θ_{ik} .

178 2.4 Inference and uncertainty quantification

179 This allows us to calculate the gradient of the posterior distributions with respect to each param-
180 eter. We can hence use efficient optimisation algorithms, such as BFGS, to optimise the posterior
181 distributions.

182 This approach also allows us to control for over-fitting by adjusting the constraint on the parame-
183 ters, which is controlled by the standard deviation of the parameter prior distributions, δ_j . This can
184 be used to control the degree of non-linearity in the response, but also to eliminate specific variables
185 from the model by constraining their parameters to be close to zero. We identify the appropriate
186 degree of constraint δ_j on NODE parameters via cross-validation. We train the NODE model on
187 the first half of the interpolated data and we predict the remaining half. We repeat this process for
188 various values of δ_j .

189 Finally, we estimate uncertainty in parameter values through anchor sampling, which produces ap-
190 proximate Bayesian estimates of the posterior distribution of the parameters (Pearce et al. 2018).
191 The technique is simple in that it requires sampling a parameter vector from the prior distribu-
192 tions, and then optimising the posterior distribution from this starting point. By repeatedly taking
193 samples, the sampled distribution approaches the posterior distribution and provides estimates and
194 error around the quantities that can be derived from the models. The expectation of the quantities
195 can then be approached by computing the mean of the approximated posterior distributions. The
196 great strength of this approach is that it is unlikely to get stuck in local maxima and provides a
197 more robust optimisation of the posterior. In this study, we took 100 posterior samples for each

time series, namely a hundred samples for the interpolation, and another hundred for the fitting of the NODE. The initial value of the parameters were picked from a random normal distribution with parameters $\sigma \geq 0.4$, which prevented underfitting the time series. We insured that there was moderate temporal autocorrelation and normality by visualising the residuals of the models. We also insured that the results were repeatable by running the entire fitting process a second time. We did not perform cross validation of results as we were only interested in estimating effects within the time series considered, rather than predicting future time steps.

2.5 Model analysis

We analyse the shape of the per-capita growth rates to recover the interaction between the three species in the system. In particular, we look at the effect and contribution of each species to the dynamics of the other. The effect is computed as the sensitivity (i.e. the gradient) of the per-capita growth rate of a given species with respect to the density of the other species. The contribution is computed following the Geber method (Hairston et al. 2005), which comes down to multiplying the dynamics of a variable by its effects on the other variables. We further compute the importance of a species in driving the dynamics of another by computing its relative contribution compared to other species at each time step. More details on how to recover these quantities can be found in our previous study (Bonnaffé, Sheldon, and Coulson 2021).

215 **3 Case study**

216 **3.1 System**

217 We consider a three-species laboratory microcosm consisting of an algal prey (*Chlorella autroph-*
218 *ica*), a flagellate intermediate predator (*Oxyrrhis marina*), and a rotifer top predator (*Brachionus*
219 *plicatilis*). The algal prey is consumed by the intermediate and top predator, the top predator also
220 consumes the intermediate predator (Arndt 1993). The dynamics of this system, here the daily
221 change in the density of each species, were recorded in three replicated time series experiments
222 performed by Hiltunen and colleagues (Hiltunen et al. 2013, Fig. 1). The aim of their experiment
223 was to determine which type of population dynamics would arise in a system with two predators
224 competing for the same resource (the algae), where one predator (the rotifer) would also be able to
225 consume its competitor (the flagellate). According to their expectations, they found prey-predator
226 oscillations, where the lag between the density peaks of each species reflected their position in the
227 food web. Namely that the peak of algae preceded the flagellate peak, which itself preceded the
228 rotifer peak.

229 Their microcosms are close to true replicates in that environmental conditions, namely temperature,
230 salinity, and nutrient influx, were maintained constant, and initial conditions, that is the initial
231 density of each species, were shared across all replicates. In spite of that, they still found evidence
232 for algae evolution in some parts of the time series, which resulted in a shift of the dynamics from
233 fast prey-predator cycles to slower oscillations, similar to those documented in previous studies on
234 similar systems (Yoshida et al. 2003; Becks et al. 2010), even in lineages where genetic variation in

235 predator defense traits was eliminated at the start of the experiment. Consequently, the time series
236 that they reported are the ones that did not present evidence of evolution, and therefore displayed
237 purely ecological dynamics.

238 We use their time series because they describe a simple yet biologically realistic ecosystem, and
239 because the quality of the replication of their microcosm reduces as much as possible observational
240 and experimental error, and rules out environmental variation (Hiltunen et al. 2013). We digitised
241 these time series by extracting by hand the coordinates of every points in the referential of the axis
242 of the graph of the original study, and analysed them.

243 **3.2 Model specifications**

244 The aim of the modelling approach is to infer the drivers of the dynamics of each species from
245 the time series data. More specifically, we want to quantify the effect of a change in the density
246 of one species on the dynamics of the other species. In this way we can understand which, and
247 to what extent, species interactions drive population dynamics. To do this we use neural ordi-
248 nary differential equation (NODEs), which is a novel methodology allowing us to infer dynamical
249 processes non-parametrically from time series data (Bonnaiffé, Sheldon, and Coulson 2021). We
250 choose this methodology over traditional approaches because it offers two advantages. The first
251 lies in the fact that NODEs approximate the dynamics of populations non-parametrically, and are
252 therefore not subject to incorrect model specifications (Jost and Ellner 2000; Adamson and Moro-
253 zov 2013). This is important as it offers an objective estimation of the inter-dependences between

state variables, and hence a reliable assessment of whether a species is contributing to the dynamics of another. The second advantage is that it is a dynamical systems approach, which means that the effects are estimated in a dynamically consistent system of ODEs (Bonnaiffé, Sheldon, and Coulson 2021). This is useful because it accounts for the dynamical nature of the system, so that it includes lag effects, not just direct correlations between variables.

We define a simple NODE system for the three-species system described previously

$$\begin{aligned}\frac{dR}{dt} &= r_R(R, G, B, \beta_R)R \\ \frac{dG}{dt} &= r_G(R, G, B, \beta_G)G \\ \frac{dB}{dt} &= r_B(R, G, B, \beta_B)B\end{aligned}\tag{9}$$

where dR/dt , dG/dt , and dB/dt denote the change in rotifer (R), algae (G), and flagellate (B) density in continuous time. The per-capita growth rates r_R , r_G , and r_B are non-parametric functions of the density R , G , B of each species. The shapes of the non-parametric functions are controlled by the parameter vectors β_R , β_G , and β_B . Fitting the NODE system (1) amounts to finding the parameter vectors, and thereby the per-capita growth rates, that best describe the changes in density observed in the time series data.

Each non-parametric functions is an artificial neural network (ANN). ANNs are powerful mathematical objects that can be trained to approximate the shape of dynamical processes (Funahashi and Nakamura 1993; Chen and Chen 1993). For the sake of simplicity, we consider the simplest form

269 of an ANN which contains a single hidden layer, namely a single layer perceptron (SLP)

$$r_R = \sum_{i=1}^N \beta_i f_{\sigma} (\beta_{i0} + \beta_{i1}R + \beta_{i2}G + \beta_{i3}B) \quad (10)$$

270 which takes as input the density of each species R , G , and B , and output the corresponding per-
 271 capita growth rate. The parameter vector β_R , β_G , β_B , contain the weight of the connections in the
 272 ANNs. The SLP can be viewed as a weighted sum of basis functions f_{σ} of the state variables of
 273 the system. In this study we consider sigmoid basis functions, as they are commonly used and
 274 their capacity to approximate any continuous function is well established theoretically (Funahashi
 275 and Nakamura 1993). The number of units in the hidden layer N is chosen to be 10, as this is
 276 a commonly used number for systems of that size (e.g. Wu, Fukuhara, and Takeda 2005). More
 277 details regarding these models can be found in our previous work (Bonnaffé, Sheldon, and Coulson
 278 2021).

279 **4 Results**

280 We analyse sequentially the dynamics of each species, focussing on the amount of variation in
 281 per-capita growth rates explained by the NODE model, the overall direction, consistency, and im-
 282 portance of ecological interactions, and differences across replicates. Results are summarised in
 283 Table 1 and described in details for each species in the following section.

284 **Drivers of top predator dynamics**

Figure 2 presents the drivers of the dynamics of rotifer. The NODE approximation of the per-capita growth rate fits quite well the interpolated per-capita growth rate across all replicates (Fig. 2, A2 B2 and C2, $r^2 > 0.7$, Table 1). The analysis of effects reveals overall a positive effect of algae on rotifer growth in all replicates (Fig. 2, A3, B3, C3, green line). The intermediate predator has a positive effect on rotifer growth in replicates A and C only (Fig. 2, A3, B3, C3, blue line). We find positive intra-specific density-dependence in the first replicate only (Fig. 2, A3, red line). Overall, all effects are consistent throughout the time series. The algae is the dominant driver of rotifer dynamics as it accounts for 55%, 93%, and 74% of the change in per-capita growth rates across the three replicates (Table 1, Fig. 2, A5, B5, C5, green line).

Drivers of the prey dynamics

The per-capita growth rate of the algae is well explained by the NODE approximation (Fig. 3, A2, B2, C2, $r^2 > 0.8$, Table 1). Overall, rotifers have a negative impact on the growth of algae in all replicates (Fig. 3, A3, B3, C3, red line). We find evidence for negative density-dependence in replicate A and positive density-dependence in replicate B, but not in replicate C (Fig. 3, A3, B3, C3, green line). The intermediate predator has an overall negative effect on Algae only in replicate B (Fig. 3, B3, blue line). The main driver of algae dynamics is the rotifer population, which accounts for 58%, 44%, and 90% of the change in algae per-capita growth rate across the three replicates. Density-dependence, however, plays a role in replicate A and B, with 40% and 24% of total change in growth, respectively (Table 1). The intermediate predator contributes only to algae growth in replicate B, accounting for 32% change in growth (Table 1). Overall, effects are

found to be consistent throughout the time series except in replicate B (Fig. 3, B3), where effects vary in complicated ways, leading to a period in the time series where the algae is mostly driven by the intermediate predator and positive density-dependence, and less impacted by the top predator (Fig. 3, B5, from time 3 to 7.5).

Drivers of the intermediate predator dynamics

The per-capita growth rate of the intermediate predator is quite well captured by the NODE approximation (Fig. 4, A2, B2, C2, $r^2 > 0.7$, Table 1). The intermediate predator is mainly negatively affected by the rotifer population (Fig. 4, A3, B3, C3, red line). The algae has a negative effect on flagellate growth in replicate A, and a positive one in replicate B (Fig. 4, A3, B3, green line). The rotifer predator dynamics accounts for 78%, 62%, 91% of the change in the flagellate growth rate, and the algae 20% and 37% in replicate A and B, respectively (Table 1, Fig. 4, A5, B5, C5). Overall, effects are consistent throughout the time series.

5 Discussion

Our ability to generalise dynamical processes and patterns across populations and communities is limited by the complexity of the processes, differences in environments, and incomplete and/or erroneous observations. It remains unclear to what extent generalisation would be possible if we overcame these limitations. We tackle this question by looking at the consistency of dynamical patterns across three replicated runs of a simple three-species community, hosted in identical environmental conditions in the lab. We expected to find consistency in the drivers of population

324 dynamics, both in time and across replicates, and thereby demonstrate that generalisation of dy-
 325 namical processes may be possible if the system states were well-observed and environmental
 326 conditions were known. To verify this expectation we (1) characterised the amount of variation in
 327 per-capita growth rates that is explainable deterministically, (2) quantified the direction, strength,
 328 and importance of ecological interactions for the growth of each population, and (3) described how
 329 these varied in time and across replicates. Our results are summarised in Figure 5. We find that
 330 only the effect of algae on rotifer ($G \rightarrow R$), and that of rotifer on algae ($R \rightarrow G$) and flagellate
 331 ($R \rightarrow B$) are conserved across the replicates. We find strong variation in the direction and impor-
 332 tance of intra-specific density-dependence in rotifer ($R \rightarrow R$) and algae ($G \rightarrow G$) growth across the
 333 three replicates. The role played by the intermediate predator in the system was also different in
 334 all replicates, in that it only contributed substantially to the dynamics of the algae in replicate B
 335 ($B \rightarrow G$), and was either negatively, positively, or not affected by the algae ($G \rightarrow B$). Overall, this
 336 shows that the dominant interactions are conserved across replicates, but that minor interactions
 337 vary substantially in importance and effect. Furthermore, we find that these dynamical processes
 338 are more consistent in time within a system, than across replicates. Our results demonstrate that
 339 because of partially generalisable dynamical processes, dynamical patterns may not be generalis-
 340 able across systems, even with limited observation error and when environmental conditions and
 341 community structure are conserved.

342 Overall, our results are consistent with the biology of the system. The rotifer top-predator is found
 343 to have a strong negative impact on the two other species, in spite of variation in prey preference

344 across replicates. This is consistent with previous study which have established the importance
345 of rotifers for top-down control of flagellate and algal populations (Arndt 1993; Hiltunen et al.
346 2013). What is more suprising is the positive intra-specific density-dependence in the growth rate
347 of the rotifer population in replicate A. This implies that the population of rotifer grows more at
348 high density. This might be explained by various biological mechanisms, such as cannibalism
349 (Gilbert 1976), though evidence remains limited in the *Brachionus* genus, or higher mating success
350 at high density (Snell and Garman 1986). Similarly, the algae shows signs of positive intra-specific
351 density-dependence in replicate B, though this effect remains confined to a brief period in the time
352 series. This may be due to a higher chance of evading predators at high-density. This shows that the
353 NODEs approach used here recovers results consistent with existing knowledge, but also identify
354 subtle, more intriguing dynamical processes.

355 What might be the drivers of differences in the dynamical processes across these three replicates?
356 One of the main source of variation in dynamics may be differences in the intrinsic structure of
357 populations, such as variation in traits influencing intra- and inter-specific interactions which may
358 lead to different dynamics (Yoshida et al. 2003; Yoshida et al. 2007; De Meester et al. 2019;
359 Bruijning, Jongejans, and Turcotte 2019). Differences in the phenotypic structure may be due to
360 unaccounted variation in initial conditions (Becks et al. 2010), or variation that developed through-
361 out time as a result of evolution (e.g. Yoshida et al. 2003; Yoshida et al. 2007). In particular, the
362 algae in this system is prone to evolve a predator defence behaviour, by forming clumps, which
363 reduce predation risk (Yoshida et al. 2003; Hiltunen et al. 2013). In their original paper, the authors

364 limited the initial genetic diversity in the algae and focussed on replicates which did not display
365 evidence of evolution, in an attempt to limit the impact of initial variation in phenotypic structure,
366 and of evolution, on the dynamics (Hiltunen et al. 2013). In spite of that, evolution may not be
367 eliminated completely, thus variation in traits governing the interactions between the species in
368 the system may still have developed during the experiment, and led to changes in the dynamical
369 processes across replicates. This would further be consistent with results from Yoshida and col-
370 leagues, who showed that evolution of prey defense could lead to ecological dynamics inconsistent
371 with the known trophic interactions (Yoshida et al. 2007). Becks and colleagues also showed that
372 small changes in the initial genotypic diversity could lead to drastically different eco-evolutionary
373 dynamics (Becks et al. 2010). Our study hence reinforces the idea that rapid evolution may prevent
374 generalisation of dynamical processes (Ezard, Côté, and Pelletier 2009; De Meester et al. 2019),
375 and further suggests that this may also be the case in simple systems with limited environmental
376 variation and opportunity for evolution.

377 Alternatively, stochasticity may be a major driver of differences across systems (Dallas et al. 2021).
378 First, stochasticity in initial conditions, arising from the sampling of the communities of each
379 replicate, could introduce differences in the interactions between the three populations. Second,
380 stochasticity in the population dynamics themselves may result in different changes in density lev-
381 els in communities that are otherwise identical. Because our modelling approach is deterministic,
382 it does not directly provide an estimate of the total variation explained by stochasticity. Our mod-
383 elling approach decomposes the variation in the data into observation and process error (Calder et

al. 2003). First, the interpolation step introduces residual observation error, namely variation that is not captured by the interpolation. Second, the fitting of the NODE to the interpolation introduces residual process error, which is variation in the observation model that is not explained by the process modelled by the NODE. Stochasticity in the dynamics could explain the observation and process residual error (Calder et al. 2003), while stochasticity in initial conditions can only influence differences across replicates. Yet, we find relatively small process and observation error ($> 70\%$ of variance explained). So that, the dynamics of the three species are well explained by relatively simple linear deterministic effects between the state variables, which means that though dynamical processes differ across replicates they are reasonably consistent in time within each system. This suggests that stochasticity in dynamics plays a minor role in driving differences in dynamics across replicates, compared to stochasticity in initial conditions. In order to quantify this, we would need to estimate the influence of stochasticity directly. This can be done by modelling explicitly the random distribution of model parameters that underpin the dynamics of populations, which would then inform us about the importance of stochasticity driven by variation at the individual-level (Fox and Kendall 2002). Additionally, we could model stochasticity explicitly in the model with neural stochastic differential equations, which would allow us to separate the amount of change explainable by the deterministic part of the model, from demographic stochasticity, at each time step (Jia and Benson 2019).

Finally, we cannot exclude the potential contribution of unobserved variables that were not monitored during the experiment, such as variation in nutrient levels in the chemostat, and which may

also lead to differences in the predation and intra-specific interactions across systems (e.g. Bonsall, Van Der Meijden, and Crawley 2003; Fussmann and Blasius 2005; Posey, Alphin, and Cahoon 2006).

Should we expect limited generalisability of dynamics across systems, even if the complexity of the process is properly captured, environmental conditions known, and the system well-observed? A similar study, that inferred dynamical processes consistency from replicated time series of a simple rotifer system, found substantial variation in vital rates across replicates (Rosenbaum et al. 2019), also pointing at a low generalisability of dynamical processes. Yet, the level of replication of the time series of their studies was not as stringent as that of the time series we considered, which leaves room for variability in dynamics to be caused by differences in experimental setup, population history, initial densities. Bruijning and colleagues also found substantial variation in vital rates across clones in a replicated system of aphids, showing that slight phenotypic variations can change the population dynamics, all else being equal (Bruijning, Jongejans, and Turcotte 2019). This phenomenon is likely to be even more important in more complicated systems and in a natural setting where most variables are unobserved, which poses a problem for the generalisation of results across studies and systems (De Meester et al. 2019). How can we expect to generalise dynamics across real systems if we are not able to do so in artificial systems? Overall, our study reinforces the view that general inferences should not be drawn from a single system, and that more efforts are required to distinguish dynamical patterns that are conserved across systems from idiosyncratic ones.

424 Can we trust our models then if they are doomed to provide partly idiosyncratic answers? Our
425 study demonstrates that processes can vary substantially across replicates, so that there may hence
426 not be a single suitable functional form and parametrisation to model them (Lawton 1999). Yet,
427 most of the work to date has involved fitting parametric models to time series data (e.g. Bruijning,
428 Jongejans, and Turcotte 2019; Pontarp, Brännström, and Petchey 2019; Rosenbaum et al. 2019),
429 which provide a very narrow view of the range of possible functions to describe the biological
430 processes at play (Jost and Ellner 2000; Adamson and Morozov 2013). These models are subjective
431 by nature (Jost and Ellner 2000; Adamson and Morozov 2013), and hence not generalisable, so that
432 they greatly reduce our chance at identifying dynamical processes that are idiosyncratic, and those
433 that are transferable.

434 What alternatives do we have then? We propose that NODEs are a suitable framework to study
435 dynamical processes, as they produce inferences that are free of model assumption and facilitate
436 comparison across studies and systems (Bonnaiffé, Sheldon, and Coulson 2021). In this sense, our
437 study already provides a potentially more objective depiction of dynamical processes than previous
438 work with parametric models. Furthermore, in this paper we overcame the practical challenges
439 of implementing NODEs by providing a computationally efficient fitting procedure, relying on
440 time series interpolation, and developed a model selection criterion robust to overfitting. Similar
441 approaches have been proposed in the past, for instance Ellner and colleagues developed a method
442 called gradient matching where they interpolated the data with cubic splines to which they fitted
443 the differential equations (Jost and Ellner 2000; Ellner, Seifu, and Smith 2002). Wu and colleagues

also relied on data interpolation of the data with ANNs to fit non-parametric approximations of population vital rates (Wu, Fukuhara, and Takeda 2005). But the approaches were too challenging and cumbersome to be implemented routinely, and were not used to tackle ecological interactions. Overall, our work demonstrates the usefulness of NODEs for inferring ecological interactions from count time series, which could readily be applied to a substantial pool of time series data.

Conclusion

Generalising dynamics across biological systems is hard because of the complexity of the dynamical processes (e.g. ecological interactions), differences in environmental context, and monitoring limitations. It remains unclear whether we could generalise dynamics if we properly modelled complexity, controlled for environmental effects, and observed systems precisely. We addressed this question by looking at the generalisability of dynamical processes across three replicated time series of a three-species system, using the novel framework of NODEs. We found that only the dominant interactions were conserved across the three time series, namely that between the algae and the rotifer, while the role of the intermediate predator varied substantially. Our results hence suggest that generalisation may not seem possible, even in simple system with no environmental variation. Given previous work in this system, the main cause of differences across replicates may be evolution in prey defence traits. We conclude that more work is required, using NODEs, to identify dynamical patterns that are conserved and those that are idiosyncratic across a wider range of systems.

Acknowledgments

464 We thank warmly the Ecological and Evolutionary Dynamics Lab and Sheldon Lab Group at the
465 department of Zoology for their feedback and support. We thank Ben Sheldon for insightful sug-
466 gestions on early versions of the work. The work was supported by the Oxford-Oxitec scholarship
467 and the NERC DTP.

468 **Data accessibility**

469 All data and code will be made fully available at <https://github.com/WillemBonnafe/NODER/rotifer>.

470 **Statement of authorship**

471 Willem Bonnaff  designed the method, performed the analysis, wrote the manuscript; Tim Coulson
472 led investigations, provided input for the manuscript, commented on the manuscript.

473 **References**

- 474 Adamson, M. W. and A. Y. Morozov (2013). “When can we trust our model predictions? Un-
475 earthing structural sensitivity in biological systems”. In: *Proceedings of the Royal Society A:*
476 *Mathematical, Physical and Engineering Sciences* 469.2149, pp. 1–19.
- 477 Arndt, H. (1993). “Rotifers as predators on components of the microbial web (bacteria, heterotrophic
478 flagellates, ciliates) - a review”. In: *Hydrobiologia* 255-256.1, pp. 231–246.
- 479 Becks, L., S. P. Ellner, L. E. Jones, and N. G. J. Hairston (2010). “Reduction of adaptive ge-
480 netic diversity radically alters eco-evolutionary community dynamics”. In: *Ecology Letters* 13.8,
481 pp. 989–997.

482 Becks, L., S. P. Ellner, L. E. Jones, and N. G. J. Hairston (2012). “The functional genomics of
 483 an eco-evolutionary feedback loop: Linking gene expression, trait evolution, and community
 484 dynamics”. In: *Ecology Letters* 15.5, pp. 492–501.

485 Bonnaiffé, W., A. Danet, S. Legendre, and E. Edeline (2021). “Comparison of size-structured and
 486 species-level trophic networks reveals antagonistic effects of temperature on vertical trophic
 487 diversity at the population and species level”. In: *Oikos* 130.8, pp. 1297–1309.

488 Bonnaiffé, W., B. C. Sheldon, and T. Coulson (2021). “Neural ordinary differential equations for
 489 ecological and evolutionary time series analysis”. In: *Methods in Ecology and Evolution* 2, pp. 1–
 490 46.

491 Bonsall, M. B., E. Van Der Meijden, and M. J. Crawley (2003). “Contrasting dynamics in the same
 492 plant-herbivore interaction”. In: *Proceedings of the National Academy of Sciences of the United
 493 States of America* 100.25, pp. 14932–14936.

494 Bruijning, M., E. Jongejans, and M. M. Turcotte (2019). “Demographic responses underlying eco-
 495 evolutionary dynamics as revealed with inverse modelling”. In: *Journal of Animal Ecology* 88.5,
 496 pp. 768–779.

497 Calder, C., M. Lavine, P. Müller, and J. S. Clark (2003). “Incorporating multiple sources of stochas-
 498 ticity into dynamic population models”. In: *Ecology* 84.6, pp. 1395–1402.

499 Cawley, G. C. and N. L. C. Talbot (2007). “Preventing over-fitting during model selection via
 500 bayesian regularisation of the hyper-parameters”. In: *Journal of Machine Learning Research* 8,
 501 pp. 841–861.

502 Chen, T. and H. Chen (1993). “Approximations of Continuous Functionals by Neural Networks
503 with Application to Dynamic Systems”. In: *IEEE Transactions on Neural Networks* 4.6, pp. 910–
504 918.

505 Dallas, T., B. A. Melbourne, G. Legault, and A. Hastings (2021). “Initial abundance and stochas-
506 ticity influence competitive outcome in communities”. In: *Journal of Animal Ecology*, pp. 1–
507 26.

508 De Meester, L. et al. (2019). “Analysing eco-evolutionary dynamics—The challenging complexity
509 of the real world”. In: *Functional Ecology* 33.1, pp. 43–59.

510 Demyanov, V., S. N. Wood, and T. J. Kedwards (2006). “Improving ecological impact assessment
511 by statistical data synthesis using process-based models”. In: *Journal of the Royal Statistical*
512 *Society. Series C: Applied Statistics* 55.1, pp. 41–62.

513 Ellner, S. P., Y. Seifu, and R. H. Smith (2002). “Fitting Population Dynamic Models to Time-Series
514 Data by Gradient Matching”. In: *Ecology* 83.8, p. 2256.

515 Ezard, T. H. G., S. D. Côté, and F. Pelletier (2009). “Eco-evolutionary dynamics: Disentangling
516 phenotypic, environmental and population fluctuations”. In: *Philosophical Transactions of the*
517 *Royal Society B: Biological Sciences* 364.1523, pp. 1491–1498.

518 Fox, G. A. and B. E. Kendall (2002). “Demographic stochasticity and the variance reduction ef-
519 fect”. In: *Ecology* 83.7, pp. 1928–1934.

520 Funahashi, K.-i. and Y. Nakamura (1993). “Approximation of dynamical systems by continuous
521 time recurrent neural networks”. In: *Neural Networks* 6.6, pp. 801–806.

522 Fussmann, G. F. and B. Blasius (2005). “Community response to enrichment is highly sensitive to
523 model structure”. In: *Biology Letters* 1.1, pp. 9–12.

524 Gamelon, M. et al. (2019). “Accounting for interspecific competition and age structure in demo-
525 graphic analyses of density dependence improves predictions of fluctuations in population size”.
526 In: *Ecology Letters* 22.5, pp. 797–806.

527 Gilbert, J. J. (1976). “Selective cannibalism in the rotifer *Asplanchna sieboldi*: Contact recognition
528 of morphotype and clone”. In: *Proceedings of the National Academy of Sciences* 73.9, pp. 3233–
529 3237.

530 Gross, K., A. R. Ives, and E. V. Nordheim (2005). “Estimating fluctuating vital rates from time-
531 series data: A case study of aphid biocontrol”. In: *Ecology* 86.3, pp. 740–752.

532 Hairston, N. G. J., S. P. Ellner, M. A. Geber, T. Yoshida, and J. A. Fox (2005). “Rapid evolution and
533 the convergence of ecological and evolutionary time”. In: *Ecology Letters* 8.10, pp. 1114–1127.

534 Hiltunen, T., L. E. Jones, S. P. Ellner, and N. G. J. Hairston (2013). “Temporal dynamics of a simple
535 community with intraguild predation: an experimental test”. In: *Ecology* 94.4, pp. 773–779.

536 Jia, J. and A. R. Benson (2019). “Neural jump stochastic differential equations”. In: *Advances in*
537 *Neural Information Processing Systems* 32.NeurIPS.

538 Jost, C. and S. P. Ellner (2000). “Testing for predator dependence in predator-prey dynamics: A
539 non-parametric approach”. In: *Proceedings of the Royal Society B: Biological Sciences* 267.1453,
540 pp. 1611–1620.

541 Kendall, B. E. et al. (2005). “Population cycles in the pine looper moth: Dynamical tests of mech-
542 anistic hypotheses”. In: *Ecological Monographs* 75.2, pp. 259–276.

543 Lawton, J. H. (1999). “Are There General Laws in Ecology ?” In: *Oikos* 84.2, pp. 177–192.

544 Pearce, T., F. Leibfried, A. Brintrup, M. Zaki, and A. Neely (2018). “Uncertainty in Neural Net-
545 works: Approximately Bayesian Ensembling”. In: *arXiv*, pp. 1–10.

546 Pontarp, M., Å. Brännström, and O. L. Petchey (2019). “Inferring community assembly processes
547 from macroscopic patterns using dynamic eco-evolutionary models and Approximate Bayesian
548 Computation (ABC)”. In: *Methods in Ecology and Evolution* 10.4, pp. 450–460.

549 Posey, M. H., T. D. Alphin, and L. Cahoon (2006). “Benthic community responses to nutrient en-
550 richment and predator exclusion: Influence of background nutrient concentrations and interactive
551 effects”. In: *Journal of Experimental Marine Biology and Ecology* 330.1, pp. 105–118.

552 Raeymaekers, J. A. M. et al. (2017). “Adaptive and non-adaptive divergence in a common land-
553 scape”. In: *Nature Communications* 8.1, pp. 1–8.

554 Reznick, D. N., H. Bryga, and J. A. Endler (1990). “Experimentally induced life-history evolution
555 in a natural population”. In: *Nature* 346.6282, pp. 357–359.

556 Rosenbaum, B., M. Raatz, G. Weithoff, G. F. Fussmann, and U. Gaedke (2019). “Estimating param-
557 eters from multiple time series of population dynamics using bayesian inference”. In: *Frontiers
558 in Ecology and Evolution* 6.234, pp. 1–14.

559 Shurin, J. B., J. L. Clasen, H. S. Greig, P. Kratina, and P. L. Thompson (2012). “Warming shifts
560 top-down and bottom-up control of pond food web structure and function.” In: *Philosophical
561 transactions of the Royal Society of London. Series B, Biological sciences* 367.1605, pp. 3008–
562 17.

563 Snell, T. W. and B. L. Garman (1986). “Encounter probabilities between male and female rotifers”.
 564 In: *Journal of Experimental Marine Biology and Ecology* 97.3, pp. 221–230.

565 Thompson, C. E., E. B. Taylor, and J. D. Mcphail (1997). “Parallel Evolution of Lake-Stream
 566 Pairs of Threespine Sticklebacks (*Gasterosteus*) Inferred from Mitochondrial DNA Variation”.
 567 In: *Evolution* 51.6, pp. 1955–1965.

568 Wu, J., M. Fukuhara, and T. Takeda (2005). “Parameter estimation of an ecological system by a
 569 neural network with residual minimization training”. In: *Ecological Modelling* 189.3-4, pp. 289–
 570 304.

571 Yoshida, T., S. P. Ellner, L. E. Jones, B. J. M. Bohannan, R. E. Lenski, and N. G. J. Hairston (2007).
 572 “Cryptic population dynamics: Rapid evolution masks trophic interactions”. In: *PLoS Biology*
 573 5.9, pp. 1868–1879.

574 Yoshida, T., L. E. Jones, S. P. Ellner, G. F. Fussmann, and N. G. J. Hairston (2003). “Rapid evo-
 575 lution drives ecological dynamics in a predator – prey system”. In: *Nature* 424.July, pp. 303–
 576 306.

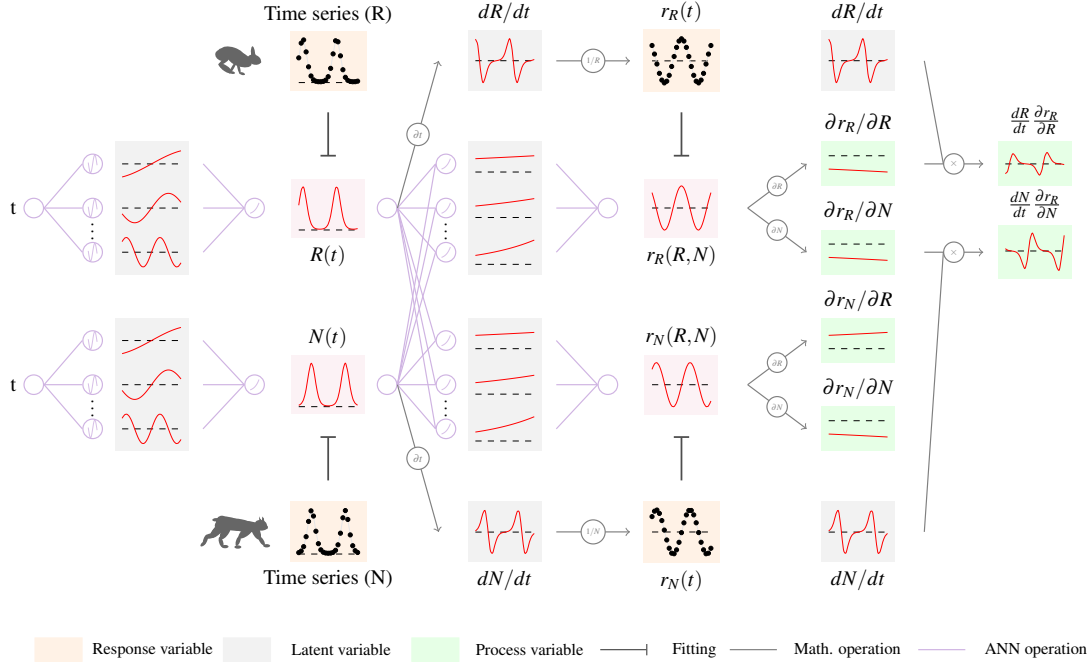


Figure 1: Overview of fitting neural ordinary differential equations by gradient matching

The first step is to compute a continuous time approximation (interpolation) of each state variables (e.g. resource $R(t)$ and predator $N(t)$). To do that we fit an ANN, that takes time as input, to each time series. Dynamics of populations can then be computed by taking the derivative of the ANN with respect to time, dR/dt and dN/dt . This provides an interpolation of the per-capita growth rate of each population, e.g. $r_R(t) = 1/R dR/dt$. In a second step, we approximate non-parametrically the per-capita growth rates with respect to the density of each populations, $r_R = s(R, N)$. To do that we fit an ANN, which takes as input the interpolated variables $R(t)$ and $N(t)$, to the interpolated per-capita growth rates $r_R(t)$ and $r_N(t)$. In a final step, we approximate the ecological interactions, by computing the sensitivity of the per-capita growth rates with respect to the density of each population, e.g. $E : N \rightarrow R = \partial r_R / \partial N$. We also compute the contribution of each species to the dynamics of the other by multiplying the dynamics of each variable with its effect on the growth rates (i.e. the Geber method), e.g. $C : N \rightarrow R = dN/dt \times \partial r_R / \partial N$.

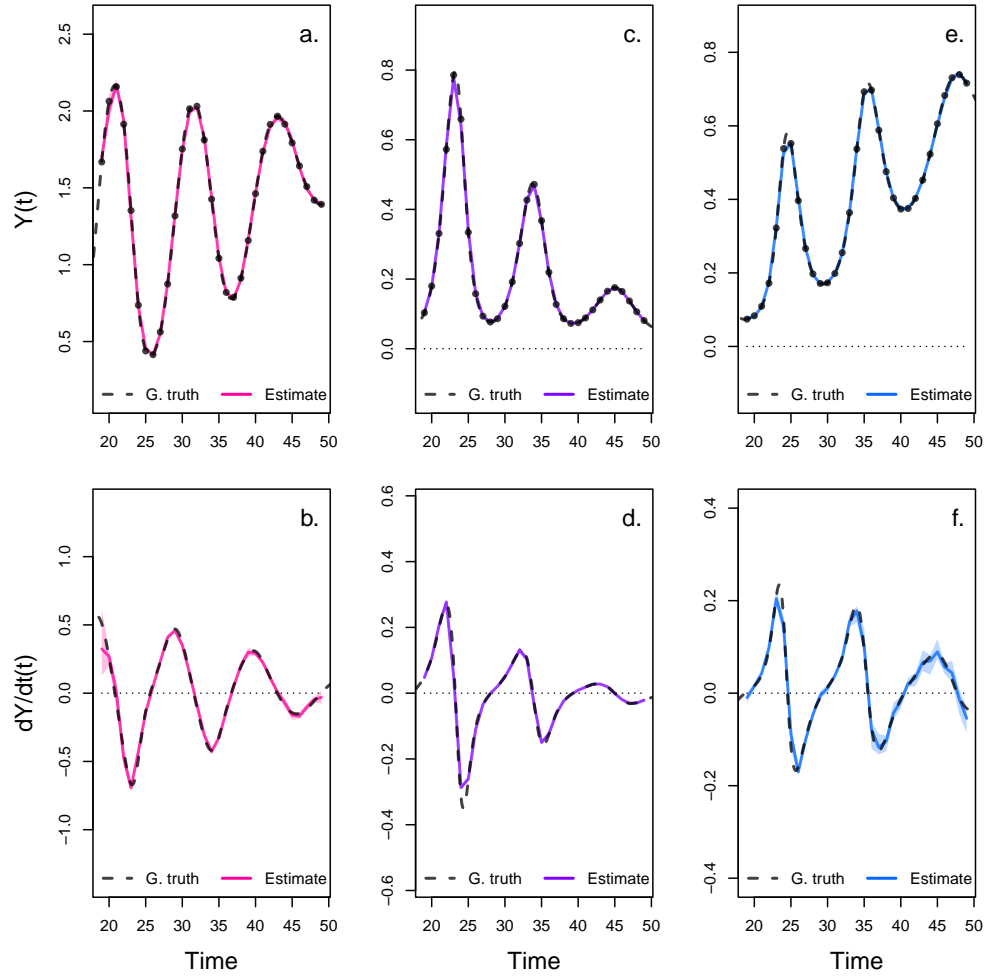


Figure 2: Interpolated density and dynamics of algae, flagellate, and rotifer in the artificial system. This figure corresponds to the first step in the overview figure. It shows the accuracy of the interpolated densities of algae (a.), flagellate (c.), and rotifer (e.). We obtain interpolated densities by fitting observed densities (black dots) with ANNs that take time as input. The observed densities were obtained by sampling a tri-trophic prey-predator ODE model at regular time steps. We then derive interpolated dynamics (b., d., f.) by computing the temporal derivative of the interpolated densities with respect to time. In all graphs, the dashed line represents the ground truth, namely trajectories generated by the ODE model. The solid lines correspond to the interpolations. The shaded area shows the 90% confidence interval, obtained by approximately sampling the marginal posterior distributions.

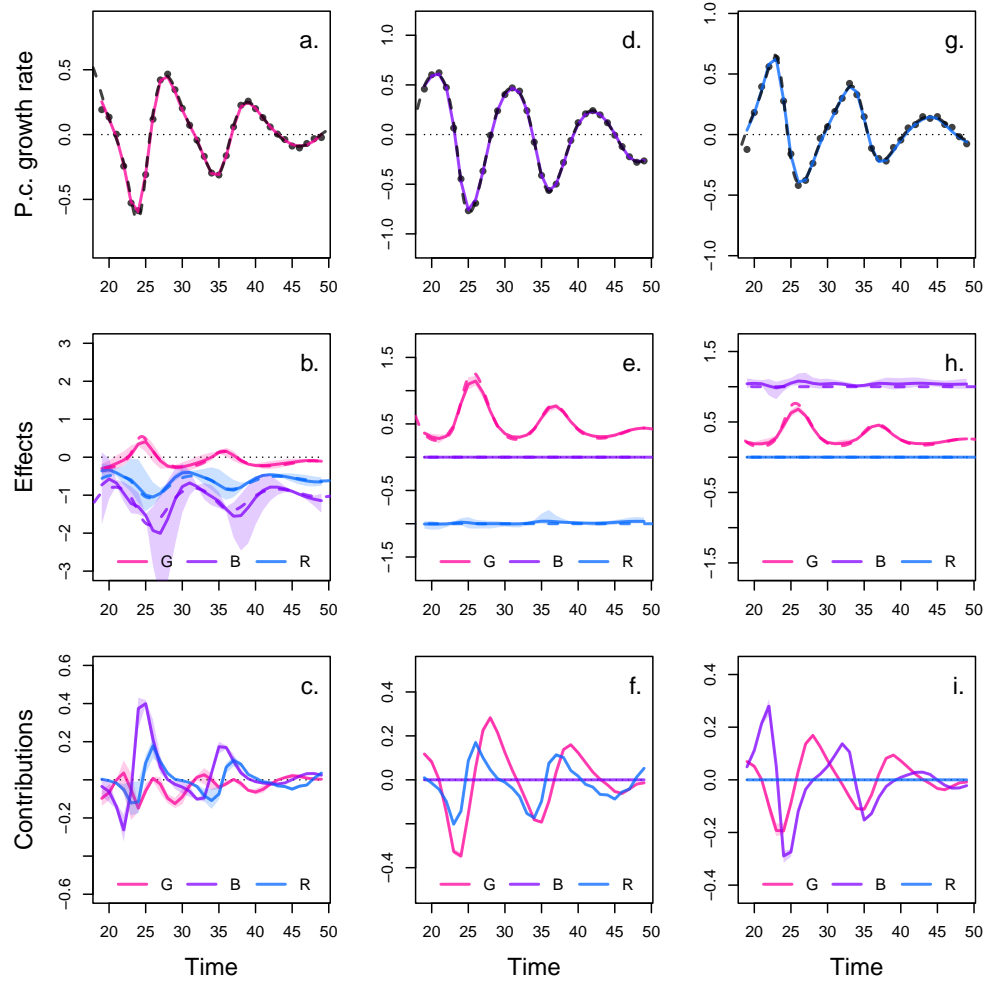


Figure 3: Drivers of dynamics of algae, flagellate, and rotifer in the artificial system. This figure corresponds to the second step in the overview figure. It displays the NODE non-parametric approximations of the per-capita growth rate of algae (a., b., c.), flagellate (d., e., f.), and rotifer (g., h., i.). We obtain the NODE approximations (a., d., g., solid line) by fitting the interpolated per-capita growth rates (black dots) with ANNs that take population densities as input. We then estimate the direction of ecological interactions (effects, b., e., h.) by computing the derivative of the NODE approximations with respect to each density. Finally, we compute the strength of ecological interactions (contributions, c., f., i.) by multiplying the interpolated dynamics of each population (fig. 1, b., d., f.) with its effects. Dashed lines correspond to ground truth, obtained from the original trajectories of the tri-trophic ODE model. The shaded area shows the 90% confidence interval, obtained by approximately sampling the posterior distributions.

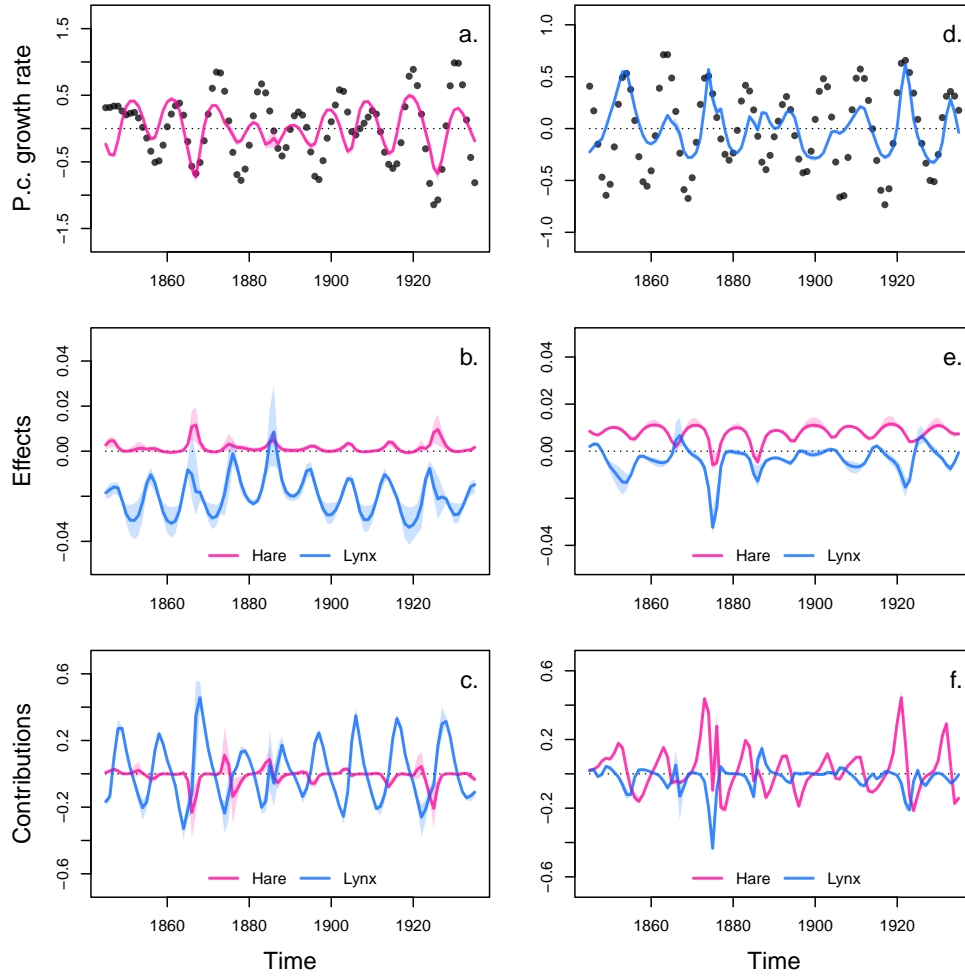


Figure 4: Drivers of dynamics of hare and lynx in the Odum and Barrett pelt count time series. This figure displays the NODE non-parametric approximations of the per-capita growth rate of hare (a., b., c.), and lynx (d., e., f.). We obtain the NODE approximations (a., d., solid line) by fitting the interpolated per-capita growth rates (black dots) with ANNs that take population densities as input. We then estimate the direction of ecological interactions (effects, b., e.) by computing the derivative of the NODE approximations with respect to each density. Finally, we compute the strength of ecological interactions (contributions, c., f.) by multiplying the interpolated dynamics of each population with its effects. The shaded area shows the 90% confidence interval, obtained by approximately sampling the posterior distributions.

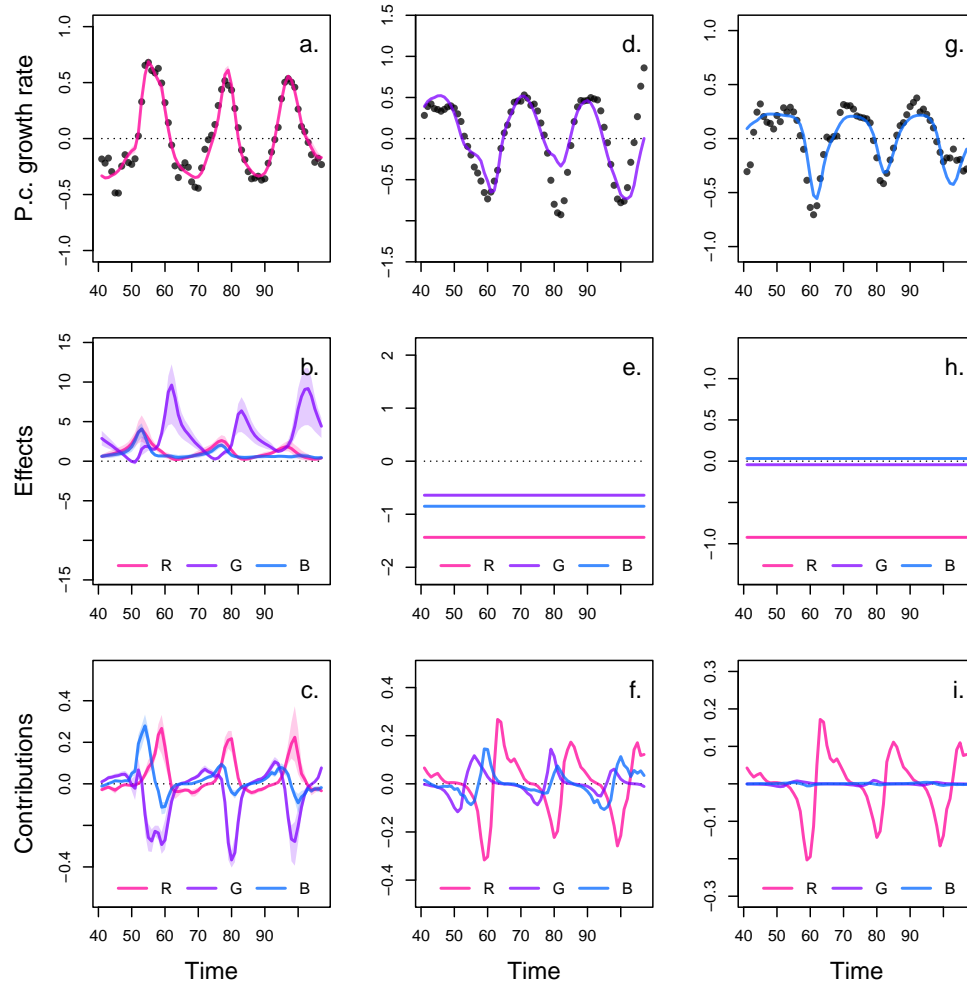


Figure 5: Drivers of dynamics of algae, flagellate, and rotifer in replicate A. This figure displays the NODE non-parametric approximations of the per-capita growth rate of algae (a., b., c.), flagellate (d., e., f.), and rotifer (g., h., i.). We obtain the NODE approximations (a., d., g., solid line) by fitting the interpolated per-capita growth rates (black dots) with ANNs that take population densities as input. We then estimate the direction of ecological interactions (effects, b., e., h.) by computing the derivative of the NODE approximations with respect to each density. Finally, we compute the strength of ecological interactions (contributions, c., f., i.) by multiplying the interpolated dynamics of each population with its effects. The shaded area shows the 90% confidence interval, obtained by approximately sampling the posterior distributions. The replicated time series were obtained by digitising the time series in Hiltunen et al. (2013).

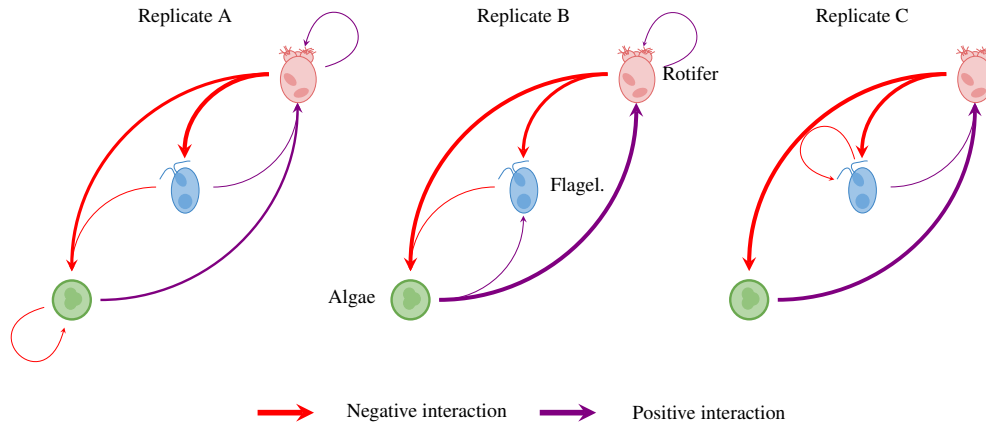


Figure 6: Interaction networks inferred from 3 replicated time series of algae, flagellate, and rotifers. This figure shows the direction and strength of ecological interactions inferred from 3 replicated sets of time series of algae, flagellate, and rotifer, using NODEs fitted by gradient matching. The replicates B and C were analysed in the same way as replicate A (see fig. 5 for details). Red and purple arrows correspond to negative or positive mean effects. We estimated mean effects by averaging effects (i.e. derivative of NODE approximated per-capita growth rates with respect to each population density) across the time series. The width of the arrows is proportional to the relative strength of the ecological interaction. We compute the relative strength as the % of total contributions attributable to either algae, flagellate, or rotifer, obtained from summing the square of contributions of each species throughout the time series. For instance in replicate A, the relative strength of the effect of rotifer on algae is found by summing the square of the red line in fig. 5 f., and computing the % of total contributions that it accounts for. We provide the value of the mean effects and relative strengths in Table 1. The replicated time series were obtained by digitising the time series in Hiltunen et al. (2013).

Table 1: Summary analysis. r^2 corresponds to the r squared of the NODE non-parametric approximation of the pre-capita growth rate compared to the interpolated per-capita growth rate for each of the three species. Mean effects are obtained by averaging the effect of one species on the growth rate of another throughout the time series. The % of total contributions is obtained by summing the square of contributions of one species density to the growth of the other at each time step throughout the time series, then by computing the proportion of total change that it accounts for.

		R	G	B
replicate A				
Mean effects	on R	0.27	0.77	0.97
	on G	-1.17	-0.44	-0.85
	on B	-0.78	0.04	0.03
% of total contributions	to R	0.08	0.48	0.44
	to G	0.75	0.08	0.17
	to B	1	0	0
replicate B				
Mean effects	on R	0.08	0.59	0.22
	on G	-1	0.05	-0.48
	on B	-0.47	0.14	-0.02
% of total contributions	to R	0.02	0.93	0.05
	to G	0.9	0	0.1
	to B	0.9	0.1	0
replicate C				
Mean effects	on R	-0.1	0.45	0.93
	on G	-1.76	-0.13	-0.12
	on B	-0.76	0.01	0.08
% of total contributions	to R	0.01	0.31	0.67
	to G	0.99	0.01	0
	to B	0.99	0	0.01

577 6 Supplementary

578 A Bayesian regularisation

579 The fitting of the models is performed in a Bayesian framework, considering normal error structure
580 for the residuals, and normal prior density distributions on the parameters

$$p(\theta|\mathcal{D}) \propto p(\mathcal{D}|\theta)p(\theta) \quad (11)$$

581 where θ is the parameter vector of the model, and \mathcal{D} the evidence, namely the data that the model
582 is fitted to. Assuming a normal likelihood for the residuals given the evidence we get

$$p(\mathcal{D}|\theta) = \prod_{i=1}^I \frac{1}{\sqrt{2\pi\sigma^2}} \exp \left\{ -\frac{e_i(\mathcal{D}, \theta)^2}{2\sigma^2} \right\} \quad (12)$$

583 where $e_i(\mathcal{D}, \theta)$ are the residuals of the model given the parameters, and the evidence. In the case of
584 the interpolation, the residuals correspond to the observation error $\varepsilon^{(o)}$ (equation 3). In the case of
585 the NODE approximation, they correspond to the process error $\varepsilon^{(p)}$ (equation 7). I is the number
586 of data points, either observations in the case of the interpolation, or interpolated points in the case
587 of the NODE fitting.

588 The prior probability density functions for the parameters are given by

$$p(\theta) = \prod_{j=1}^J \frac{1}{\sqrt{2\pi\delta_j^2}} \exp \left\{ -\frac{\theta_j^2}{2\delta_j^2} \right\} \quad (13)$$

where J is the number of parameters in the models. The parameter δ_j controls the dispersion of the priors, and thereby the complexity/level of constraint of the model.

There is no standard approach for choosing δ . Low values of dispersion may increase constraint on parameters too drastically, which would lead to underfitting, and result in a reduction of the variance of parameter estimates and bias mean estimates towards 0. In contrast, too high values of dispersion may lead to overfitting, by allowing for more complex shapes. To account for this, we optimise the models on the second-level of inference. This means that we are finding the optimal value of δ , in addition to optimising the model parameters. We do this by optimising the marginal posterior density of the parameters, obtained by averaging out δ following a modification of the approach developed by Cawley and Talbot (Cawley and Talbot 2007). This yields the following expression for the marginal log posterior density of the parameters

$$\log P(\Omega|\mathcal{D}) \propto -\frac{I}{2} \log \left(1 + \sum_{i=1}^I \left(\varepsilon_i^{(o)} \right)^2 \right) - \frac{J}{2} \log \left(1 + \sum_{j=1}^J \Omega_j^2 \right) \quad (14)$$

$$\log p(\beta|\Omega) \propto -\frac{1}{2} \sum_{i=1}^I \left(\frac{\varepsilon_i^{(p)}}{\sigma} \right)^2 - \frac{1}{2} \sum_{j=1}^J \left(\frac{\beta_j}{\delta_j} \right)^2 \quad (15)$$

which amounts to optimising the log of the sum of squared residuals rather than the sum of squared residuals. $P(\theta|\mathcal{D})$ designates the marginal posterior distribution. More details on how to derive this expression from equation (8) can be found in a supplementary file (See supplementary A).

In this section we describe how to derive the modified model selection criteria developed by Caw-

ley and Talbot (Cawley and Talbot 2007). Bayesian regularisation simply amounts to constraining
 the values of the parameters in the model to be close to a desired value. Usually, parameters are
 constrained by choosing normal priors centered about 0. In this case, the standard deviation of the
 normal priors governs the range of values that the parameters can take, and hence constrains more
 or less strongly the behaviour of the model (Cawley and Talbot 2007). Performing inference on the
 second level means that we are trying to find the appropriate value of the dispersion of the priors,
 in other words, the appropriate level of constraint on the model. In practice, choosing the level of
 constraint is difficult, Cawley and Talbot hence developed a criterion to perform model selection
 on the second level of inference. They proposed to optimise the marginal posterior distribution by
 averaging out the dispersion of the priors. With an appropriate choice of prior, the dispersion can
 be integrated out, leaving us with a formula for the posterior that only depends on the parameters
 of the model,

$$\log P(\theta|\mathcal{D}) \propto -\frac{I}{2} \log \left(\sum_{i=1}^I e_i(\mathcal{D}, \theta)^2 \right) - \frac{J}{2} \log \left(\sum_{j=1}^J \theta_j^2 \right) \quad (16)$$

where $P(\theta|\mathcal{D})$ denotes the marginal posterior density, \mathcal{D} denotes the evidence, I and J denote the
 number of data points and parameters, respectively, e_i denote the residuals of the model, and θ
 denote the parameters of the model. The construction is elegant because it is not sensitive to the
 choice of prior hyperparameters, and simple as it amounts to optimising the log of the sum of
 squares, rather than the sum of squares (in the case of normal ordinary least square).

621 The issue with this formula is that the marginal posterior density is infinity when the parameters
 622 are 0, which leads to underfitting. In this paper we use a modified criterion, which corrects for that
 623 problem

$$\log P(\theta|\mathcal{D}) \propto -\frac{I}{2} \log \left(1 + \sum_{i=1}^I e_i(\mathcal{D}, \theta)^2 \right) - \frac{J}{2} \log \left(1 + \sum_{j=1}^J \theta_j^2 \right) \quad (17)$$

624 where the marginal posterior density depends only on the residuals of the model when the parame-
 625 ters are equal to 0, and otherwise depends on both the parameters and the residuals. This construc-
 626 tion can be obtained simply by assuming a gamma prior for the parameters $p(\xi) \propto \frac{1}{\xi} \exp\{-\xi\}$,
 627 where ξ is the regularisation parameter, instead of the improper Jeffreys' prior that Cawley and
 628 Talbot used in their original study, namely $p(\xi) \propto \frac{1}{\xi}$. The details of the integration of the posterior
 629 distribution over ξ can be found in Cawley and Talbot's original paper.